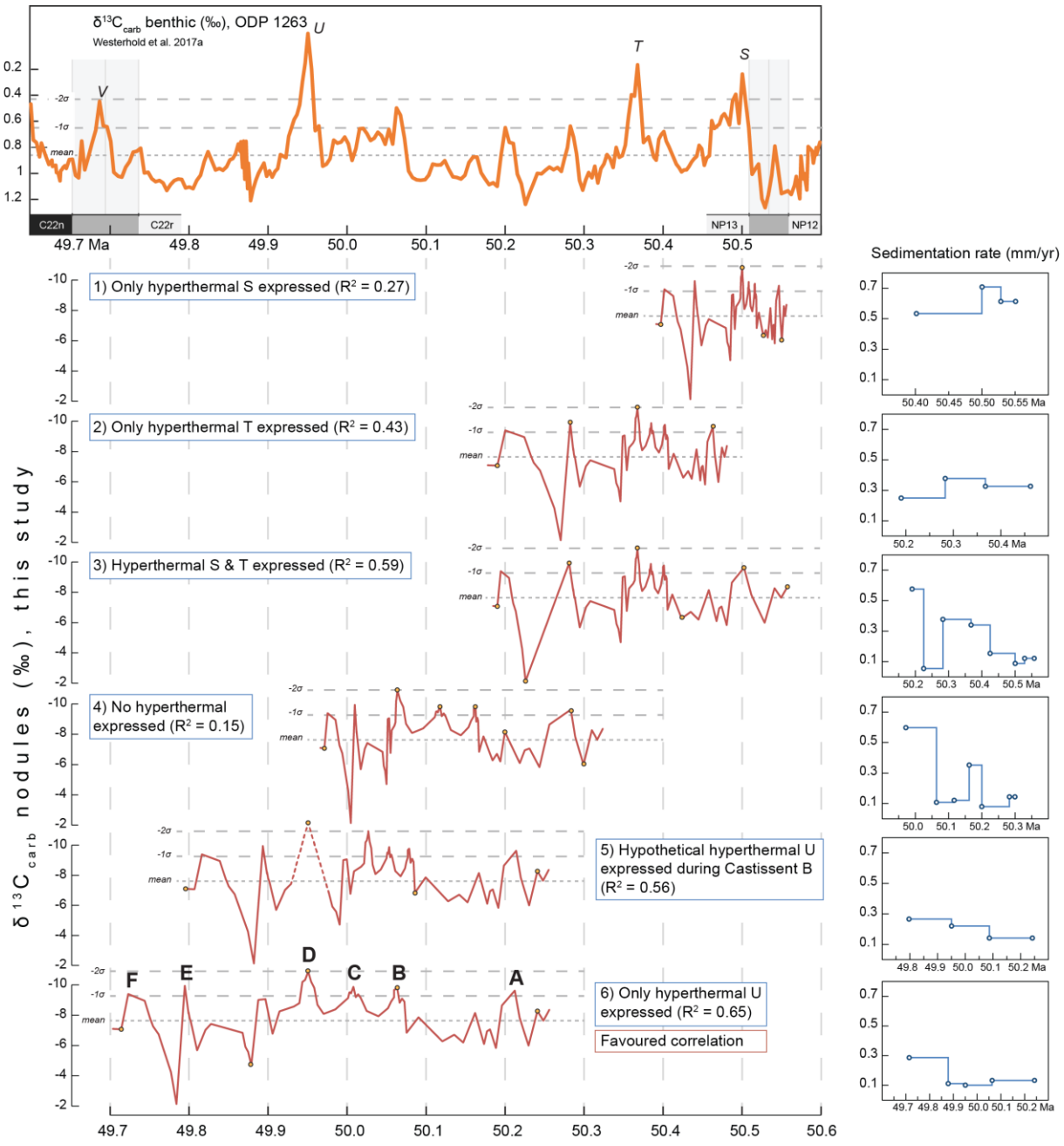

Figure S1: Correlation options 1 to 6 between $\delta^{13}C$ benthic record from site 1263 and $\delta^{13}C$ from carbonate nodules (this study) using the Analyseries software (Paillard et al., 1996). Tie-points used to correlate both curves are showed in yellow dots. Sedimentation rate in mm/yr for each option is showed on the right. Option 6 is detailed in Figure 8.

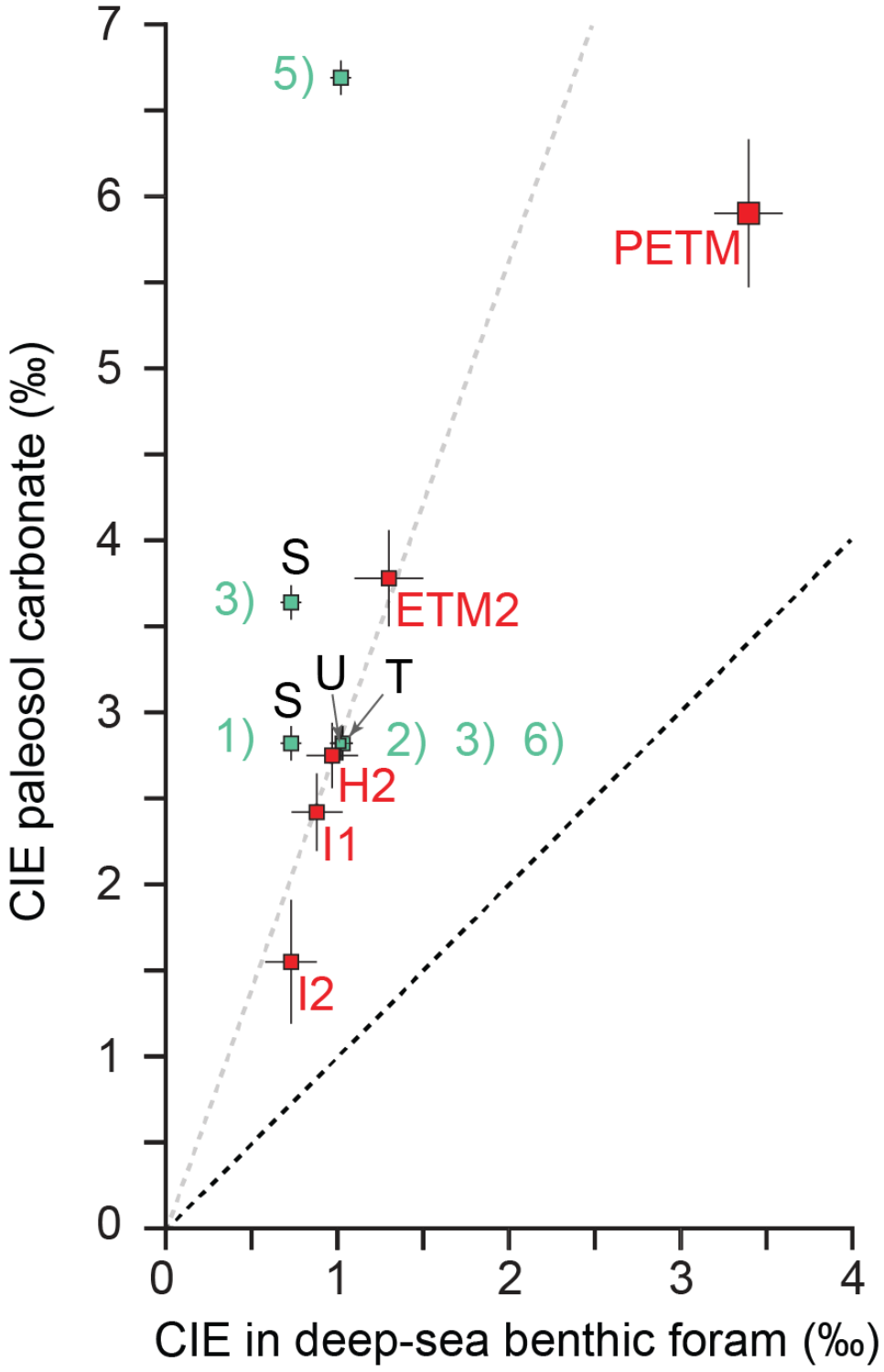

Figure S2: CIE amplitudes from I1, I2, H2, ETM2 and PETM in continental and marine environments after (Abels et al., 2016). Options 1 to 6 from Figure S1 are plotted as comparison.

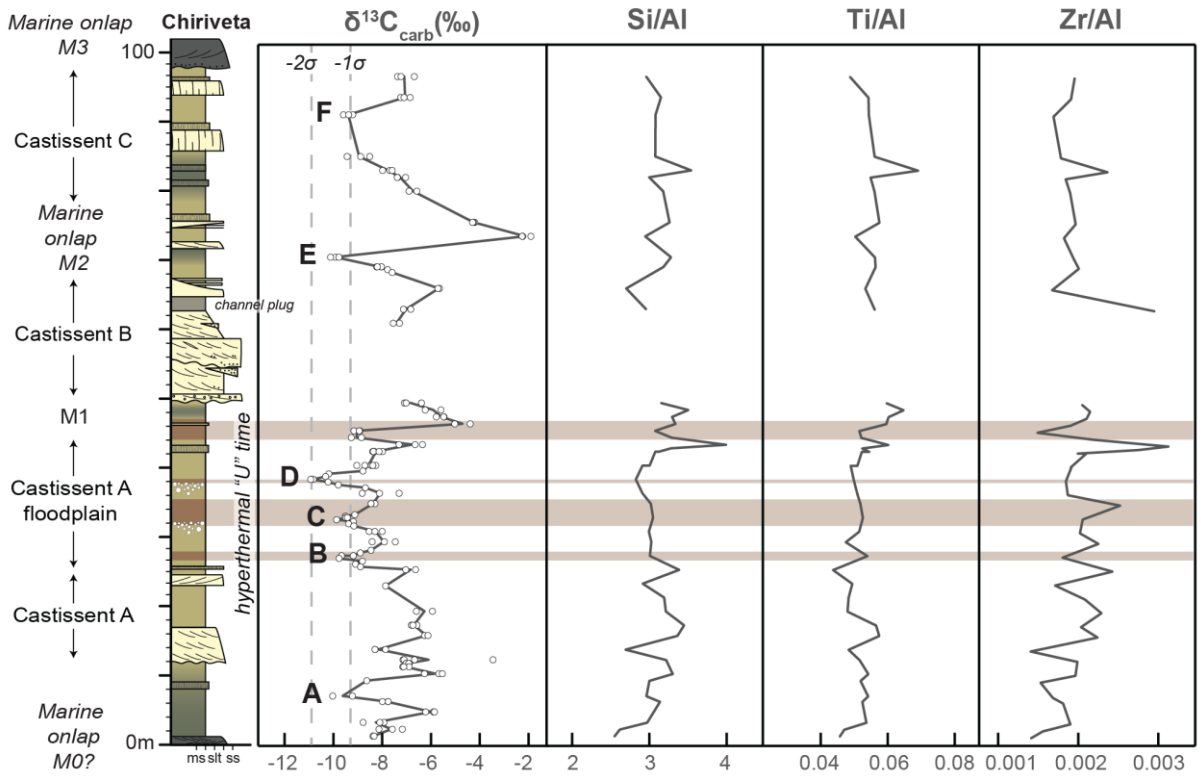

Figure S3: Chiriveta section showing $\delta^{13}C$ and grain-size proxies Si/Al, Ti/Al and Zr/Al. Al is more concentrated in the fines and Si, Ti and Zr in the coarse fraction of the sediment (Lupker et al., 2012). An increase of these ratios would suggest an increase in grain-size. Here, no direct correlation is observable between the grain size and the NCIEs.

samples	Phyllosilicates	Quartz	Feldspath-K	Plg-Na	Calcite	Indosés	Smectite	Illite-Smectite	Mica	Chlorite	Kaolinite
MO2	35.30	23.37	0.00	1.11	36.07	4.12	38.05	3.81	29.97	15.46	12.68
MO3	50.32	33.98	1.87	1.77	6.83	5.21	34.66	3.15	34.87	19.84	7.45
MO4	21.57	15.74	0.00	0.00	53.96	8.71	31.04	2.41	24.11	20.30	22.11
MO5	13.71	19.58	0.00	0.00	62.52	4.17	26.73	5.85	20.78	33.83	12.78
MO6	34.78	27.56	1.76	0.00	30.23	5.66	38.81	1.37	20.87	30.41	8.52
MO7	32.57	39.76	3.07	1.03	20.56	2.99	26.96	2.92	32.95	29.87	7.27

Table S1: Clay minerals results from sample MO2 to MO7 in the top of the Castissent Formation Member A, between 44 and 50m. From (Nicolaides, 2017).

sample	height (m)	Al (ppm)	Ti (ppm)	Fe (ppm)	Zr (ppm)
2CH21	96	35722.03886	1741.232797	13004.05365	69.80703089
2CH20	93	53399.22227	2896.887595	26241.90692	102.0027324
2CH19	90.5	62323.49447	3386.62809	28122.79949	105.4156279
2CH18	84.5	70062.92314	3928.547221	32833.31428	125.1045792
2CH17	82.5	49829.84454	3442.319098	30055.24786	117.9007775
2CH16	81.5	62653.58908	3440.134427	31770.77741	115.3843071
2CH15	79.5	59648.45808	3344.117529	30092.96791	113.202646
S093	75	37316.28923	2145.734909	19819.63077	73.4467328
S092	73	36465.96172	1834.340824	16910.80025	66.38333503
S091	70	83411.30378	4687.47299	48621.43875	162.1496165
S090	68.6	66755.91805	3762.294958	35064.37338	133.9392266
S089	65.5	52205.89985	2782.934668	19424.12216	87.26031958
S088	62.5	66016.96245	3703.888199	40550.41391	194.6909276
MO2	49	57079.9901	3407.42471	26358.369	116.9071497
MO3	48	78503.73464	5080.617227	44616.41448	168.7810022
MO4	47	38632.68297	2326.88156	23423.75105	81.21215023
MO5	46	35666.23464	2124.793449	20252.2885	67.93857857
MO6	45	67280.75429	3467.53334	36062.46073	100.2098822
MO7	44	73928.46172	3857.491095	30310.15318	161.0371853
MO8	43	40822.67569	2456.380655	22990.56997	127.6102494
MO9	42.5	61266.27103	3209.862852	22214.42571	168.4785937
MO10	42	70736.94061	3856.054765	37479.31295	141.1430283
CH13	42	77156.68224	4030.381862	37161.98495	162.0632141
MO11	40	76820.89258	3912.132013	35009.47757	146.3703747
CH12	40	70740.43406	3462.850178	28819.91624	135.4944701
CH11	38	94884.28413	4727.0264	37525.7874	175.0883788
CH10	36	75584.06579	3847.34022	23751.18468	141.2618316
CH9	34.5	72862.99592	3776.151325	31488.65732	183.8798249
CH8	32.5	98856.93697	5195.789225	44653.47795	203.2555674
CH7	30.5	64223.7492	3307.17124	29947.58776	129.7271087
CH6	29	65052.67933	3088.124771	23421.83841	146.4675774
CH5	27	91510.81252	4934.521874	47587.70576	164.9144939
CH4	25	69228.18879	3026.31427	27584.51801	168.0033804
CH3	23	90131.50029	4454.521874	46650.11893	154.1357921
CH2	21	73852.82489	3569.186931	32013.51221	153.70378
CH1	19	69157.59199	3319.120546	31197.06916	158.4127118
2CH14	17	61630.97263	3484.588259	25148.70109	125.4393886
2CH13	15.5	60996.63857	3505.107269	31762.80329	136.7149043
2CH12	13.5	67079.02576	3240.508597	30127.1862	94.20491403
2CH11	12	46807.48282	2417.816986	18984.95573	93.08168258
2CH10	10	52672.2754	2856.175465	25014.74924	103.4931741
2CH9	9	67219.21863	3487.11089	30697.52591	102.8235554
2CH8	6.8	75173.34891	4071.347462	35723.89379	126.6166216
2CH7	6	56945.40131	2984.008899	25258.15965	103.0827626
2CH6	3	47496.96608	2547.15917	20364.47805	90.30600486
2CH5	2	52020.0738	2448.148911	28009.1921	81.0825466
2CH4	1	61612.41368	2815.692664	30977.08629	86.75270537

sample	height (m)	$\delta^{13}C$ ‰ VPDB	$\delta^{18}O$ ‰ VPDB	sample	height (m)	$\delta^{13}C$ ‰ VPDB	$\delta^{18}O$ ‰ VPDB
2CH21-P1	96	-7.4	-5.2	MO5-G1	46	-4.39	-6.34
2CH21-P2	96	-7.2	-5.0	MO5-G2	46	-5.02	-6.20
2CH21-G3	96	-6.7	-6.1	MO6-P1	45	-9.16	-5.64
2CH20-P1	93	-7.2	-6.3	MO6-P2	45	-8.92	-5.65
2CH20 P2	93	-7.1	-5.4	MO6-P3	45	-8.94	-5.65
2CH20-G3	93	-6.9	-5.5	MO7-P1	44	-8.85	-5.19
2CH19-P1	90.5	-9.2	-5.7	MO7-P2	44	-9.27	-5.28
2CH19-G2	90.5	-9.6	-5.7	MO8-P1	43	-7.31	-5.89
2CH19-G3	90.5	-9.4	-5.7	MO8-P2	43	-6.65	-5.88
2CH18-P1	84.5	-8.5	-6.1	MO8-G3	43	-6.35	-5.99
2CH18-P2	84.5	-9.4	-5.9	MO10-P1	42	-8.33	-5.93
2CH18-P3	84.5	-8.9	-6.0	MO10-P2	42	-8.32	-6.06
2CH17-P1	82.5	-7.7	-6.3	MO10-P3	42	-8.39	-6.00
2CH17-P2	82.5	-8.0	-6.2	CH13-P3	42	-7.99	-5.83
2CH17-G3	82.5	-7.6	-6.4	CH13-P2	42	-8.36	-5.86
2CH16-P1	81.5	-7.4	-6.5	CH13-P1	42	-8.13	-5.39
2CH16-P2	81.5	-7.0	-6.2	MO11-P1	40	-8.45	-5.64
2CH16-G3	81.5	-7.4	-6.4	MO11-P2	40	-8.27	-5.95
2CH15-P1	79.5	-6.9	-6.5	CH12-P3	40	-8.71	-5.31
2CH15-P2	79.5	-6.6	-6.6	CH12-P2	40	-8.38	-5.84
93-P1	75	-4.2	-6.1	CH12-P1	40	-9.04	-5.16
93-P2	75	-4.3	-6.1	RB3-7	39.2	-8.79	-6.07
93-P3	75	-4.3	-6.3	RB3-6	38.8	-10.19	-5.94
92-P1	73	-1.9	-6.4	RB3-5	38.4	-10.33	-5.90
92-P2	73	-2.2	-6.4	RB3-4B	38	-10.82	-5.89
92-P3	73	-2.3	-6.4	RB3-4A	38	-10.93	-5.85
91-P1	70	-9.9	-5.7	RB3-3	37.6	-10.22	-6.01
91-P2	70	-10.1	-6.0	RB3-2	37.2	-9.80	-6.33
91-G3	70	-9.8	-6.3	RB3-1	36.8	-8.69	-6.31
90-P1	68.6	-8.0	-6.1	CH10-G3	36	-7.31	-6.24
90-P2	68.6	-8.0	-6.1	CH10-P2	36	-8.11	-5.95
90-P3	68.6	-8.2	-6.0	CH10-P1	36	-8.82	-5.93
RB4-3	68.6	-8.21	-5.50	CH9-P2	34.5	-8.29	-6.14
RB4-2	68.2	-7.78	-5.96	CH9-P1	34.5	-8.46	-6.36
RB4-1	67.8	-7.59	-6.26	RB2-7	32.9	-9.12	-6.45
89-P1	65.5	-5.7	-6.3	RB2-6	32.7	-9.51	-6.14
89-P2	65.5	-5.7	-6.4	RB2-5B	32.5	-9.50	-6.16
88-P1	62.5	-6.8	-6.2	RB2-5A	32.5	-9.43	-5.98
88-G2	62.5	-7.1	-6.1	RB2-4	32.2	-9.87	-5.75
88-G3	62.5	-7.1	-6.2	RB2-3	31.9	-9.18	-5.99
87-P1	60.5	-7.5	-6.5	RB2-2	31.6	-9.38	-5.80
87-P2	60.5	-7.3	-6.4	RB2-1	31.3	-9.16	-5.78
MO2-P1	49	-7.09	-5.56	CH7-P3	30.5	-8.53	-5.92
MO2-P2	49	-7.02	-5.69	CH7-P2	30.5	-8.00	-6.01
MO2-P3	49	-6.39	-5.82	CH7-P1	30.5	-8.30	-5.98
MO3-P1	48	-5.59	-5.97	CH6-P3	29	-8.41	-6.10
MO3-P2	48	-6.23	-5.75	CH6-P2	29	-7.46	-6.16
MO4-P1	47	-5.78	-5.12	CH6-G1	29	-7.91	-6.04
MO4-P2	47	-5.46	-5.13	RB1-7	27.8	-8.46	-6.76
MO4-P3	47	-5.48	-5.20				

sample	height (m)	$\delta^{13}C$ ‰ VPDB	$\delta^{18}O$ ‰ VPDB
RB1-6	27.4	-8.90	-6.83
RB1-5B	27	-9.19	-6.10
RB1-5A	27	-9.67	-6.01
RB1-4	26.6	-9.77	-6.01
RB1-3	26.2	-8.82	-6.17
RB1-2	25.8	-9.09	-6.35
RB1-1	25.4	-8.89	-5.95
CH4-P2	25	-6.64	-6.49
CH4-P1	25	-7.04	-6.16
CH3-P1	23	-7.86	-5.31
CH1-P2	19	-5.94	-6.06
CH1-P1	19	-6.60	-6.03
2CH14-P1	17	-6.6	-5.7
2CH14-P2	17	-6.8	-5.8
2CH14-P3	17	-6.7	-5.6
2CH13-P1	15.5	-6.3	-6.5
2CH13-P2	15.5	-6.1	-6.7
2CH12-P1	13.5	-8.3	-5.3
2CH12-P2	13.5	-8.3	-5.4
2CH12-G3	13.5	-7.9	-5.4
2CH3-P1	12	-3.5	-7.0
2CH11-P1	12	-7.1	-5.9
2CH11-P2	12	-6.7	-5.9
2CH11-G3	12	-7.1	-5.8
2CH1-P1	11.5	-6.9	-5.5
2CH1-P2	11.5	-7.0	-5.5
2CH1-P3	11.5	-6.9	-5.5
2CH2-P1	11	-7.2	-5.5
2CH2-P2	11	-6.9	-5.5
2CH2-P3	11	-7.1	-5.7
2CH10-P1	10	-5.7	-6.6
2CH10-P2	10	-5.5	-6.6
2CH10-G3	10	-6.3	-6.6
2CH9-P1	9	-8.6	-5.5
2CH8-P1	6.8	-10.0	-5.1
2CH8-P2	6.8	-9.2	-5.3
2CH7-P1	6	-8.0	-5.9
2CH7-P2	6	-7.8	-5.8
2CH7-G3	6	-7.8	-5.7
2CH6BIS-P1	4.5	-5.9	-6.5
2CH6BIS-P2	4.5	-6.2	-6.4
2CH6BIS-P3	4.5	-5.9	-6.6
2CH6-P1	3	-7.9	-6.3
2CH6-P2	3	-8.8	-6.2
2CH6-G3	3	-8.1	-6.3
2CH5-P1	2	-7.6	-6.3
2CH5-P2	2	-8.1	-6.2
2CH5-P3	2	-7.2	-6.3
2CH4-P1	1	-8.4	-6.1
2CH4-P2	1	-8.3	-6.3

Table S2: Al, Ti, Fe, Zr, $\delta^{13}C$ and $\delta^{18}O$ values of the Chiriveta section

References Supplement

Abels, H. A., Lauretano, V., van Yperen, A. E., Hopman, T., Zachos, J. C., Lourens, L. J., Gingerich, P. D. and Bowen, G. J.: Environmental impact and magnitude of paleosol carbonate carbon isotope excursions marking five early Eocene hyperthermals in the Bighorn Basin, Wyoming, Clim. Past, 12(5), 1151–1163, doi:10.5194/cp-12-1151-2016, 2016

Lupker, M., France-Lanord, C., Galy, V., Lavé, J., Gaillardet, J., Gajurel, A. P., Guilmette, C., Rahman, M., Singh, S. K. and Sinha, R.: Predominant floodplain over mountain weathering of Himalayan sediments (Ganga basin), Geochim. Cosmochim. Acta, 84, 410–432, doi:10.1016/j.gca.2012.02.001, 2012.

Nicolaides, E.: Analyses des sédiments marins et continentaux éocènes dans les Pyrénées Espagnoles, Université de Lausanne., 2017.

Paillard, D., Labeyrie, L. and Yiou, P.: Macintosh Program performs time-series analysis, Eos, Trans. Am. Geophys. Union, doi:10.1029/96EO00259, 1996.